The International Journal of Advanced Manufacturing Technology
https://doi.org/10.1007/s00170-024-13074-0

ORIGINAL ARTICLE

Prediction of weld bead geometry of AA5083 using taguchi technique: in the presence of siliconized zn-graphene oxide complex nanoparticles

Farhad Rahmati[1] · **Farhad Kolahan**[1] · **Masood Aghakhani**[2]

Received: 12 December 2023 / Accepted: 18 January 2024

Abstract
The fact that the weld geometry is vital in the cooling rate and determining the weld metal quality is obvious to all. So, the Taguchi technique was used to determine the process parameters of gas metal arc welding to access optimal weld bead geometry. In addition, this study investigated the effect of siliconized Zn-graphene oxide complex nanoparticles as one of the input parameters on the weld bead geometry, including the penetration depth, bead height, and bead width of the weld. Hence, the S/N and ANOVA statistical analyses were done to establish the relationship between the gas metal arc welding process's input parameters and output variables to achieve the weld bead with the highest penetration depth and the lowest bead height and width. The results showed that in the L00 sample compared to the L0 sample (sample without nanoparticles), in addition to having a very high penetration depth, the ultimate tensile strength, and yield strength have increased by 58.84% and 28.24%, respectively.

Keywords Nanoparticles · Aluminum alloy · Metal inert gas welding · Taguchi technique · Analysis of Variance

1 Introduction

Welding is one of the methods of joining metal materials used in various industries, ranging from shipbuilding and automobile manufacturing to nuclear and construction industries [1–3]. Welding is done with different methods, but in the meantime, shielded gas metal arc welding (GMAW) is widely used compared to other welding methods due to its features, such as high deposition rate, no need to clean slag, and high speed [4–9]. One of the cases of GMAW is in the shipbuilding industry, where aluminum alloy 5083 (AA5083) is widely used due to its properties, such as low density, good mechanical properties, and corrosion resistance [10–18]. On the other hand, during the welding process, the goal is always to create weld metal with suitable mechanical properties, good corrosion resistance, and suitable microstructures. Therefore, careful examination of the welding process, determination of appropriate parameters, research, and investigation of new ideas to achieve this goal have always been considered. Meanwhile, the use of nanoparticles and the effects that can sometimes have in improving the mechanical and microstructural properties of weld metal, as a new idea, can be a suitable option to create a more suitable weld metal. A study in this field examined the effect of siliconized zinc oxide-graphene complex nanoparticles on the microstructure and mechanical properties of AA5083 in welded metal. The results showed that the presence of graphene oxide and oxygen nanoparticles in the welding metal changed the direction of the Marangoni flow, which caused the nanoparticle-welded samples to have a much greater penetration depth than those welded without using nanoparticles. The distribution of nanoparticles throughout the welding metal and the activation of grain growth mechanisms also improved the resulting microstructures and the welding metal's mechanical properties [19]. In addition, in another study, Fatahi et al. investigated the effect

✉ Farhad Rahmati
farhadrahmati_24@mail.um.ac.ir

Farhad Kolahan
kolahan@um.ac.ir

Masood Aghakhani
aghakhani@razi.ac.ir

1 Department of Mechanical Engineering, Ferdowsi University of Mashhad, Mashhad, Iran

2 Department of Mechanical Engineering, Razi University, Kermanshah, Iran

Published online: 30 January 2024

of graphene/aluminum composite nanoparticles in welding Al6061 sheets [20]. In 2020, Khosravi et al. investigated the effect of graphene oxide and reduced graphene oxide nano sheets on the microstructure and mechanical properties of weld metal [21]. In 2016, in welding Al6061 by friction stir process, Moriya et al. investigated the mechanical properties of the weld metal by adding Graphite, Graphene, and Carbon nanotubes to the weld metal [22]. In other studies, Agakhani et al. studied the effect of Cr_2O_3 and TiO_2 nanoparticles in submerged arc welding [23, 24]. Although research on the use of nanoparticles sometimes proves the usefulness of this idea, it is essential to examine all the different aspects of a welding process. Therefore, investigating the effects of individual parameters and the interaction between parameters and using statistical analysis can be helpful for a more detailed analysis of test results, predicting the welding situation, and a correct understanding of the process. This study investigated the effects of siliconized zinc oxide-graphene complex nanoparticles as one of the input parameters, along with the two main parameters of the GMAW process, current intensity and welding speed, in joining AA5083 alloy sheets. In addition, using the Taguchi method, the optimal level for each parameter was determined. Using the obtained results, the geometry of the weld bead was predicted.

2 Taguchi method

Taguchi's technique is an efficient tool for designing high-quality manufacturing systems, and it offers a simple and systematic method for optimizing the design for different characteristics such as mechanical properties, performance, quality, and cost. To evaluate optimal parameter settings, the Taguchi method uses a statistical measure of performance called signal-to-noise ratio. The S/N ratio is the ratio of the mean (signal) to the standard deviation (noise). The ratio depends on the quality characteristics of the process to be optimized. Further, Taguchi's technique determines the most influential parameters in the overall performance. Taguchi defines three categories in only a few experiments' signal/noise ratio analyses: the lower-the-better, the larger-the-better, and the nominal-the-better. The number of experiments increases with the increase of process parameters. To solve this complexity, the Taguchi method uses a unique design of an orthogonal array to study the entire process parameter space with only a few experiments [25]. The orthogonal array provides a set of well-balanced (minimum experimental runs) experiments and Taguchi's signal-to-noise ratios, which are logarithmic functions of the desired output; and serve as objective functions for optimization. This technique helps in data analysis and prediction of optimum results [26–30]. In the design of Taguchi experiments, compared to the Full Factorial Design method, although the interaction between parameters is not considered, it can obtain a detailed view of the entire process with a minimum number of experiments and reduce costs [31, 32]. This article used the Taguchi technique to determine the effect of parameters to achieve a weld with the most increased penetration depth and the lowest amount of weld height and width. In this regard, the parameters of current intensity, welding speed, and the amount of siliconized Zn-graphene oxide complex nanoparticles were investigated, and S/N and ANOVA analyses were also used to investigate the effects of these parameters on the weld bead geometry.

3 Experimental

AA5083 samples were welded under pure argon gas protection at 20 L per minute flow rate with AWS/SFA 5.10 ERS183 filler in this research. The composition of the base metal and electrode used is shown in Table 1. Current intensity, welding speed, and the amount of siliconized Zn-graphene oxide complex nanoparticles as Taguchi's technique determined process input parameters in three levels. Table 2 shows the values of the coded input parameters. On the side edge of the samples, a longitudinal groove was created at a distance of 1 mm from the upper edge of the sheet by a universal milling machine to exploit nanoparticle powder. The samples were prepared by placing different amounts

Table 2 Input parameters at different levels

Parameter	units	Level 1	Level 2	Level 3
current intensity	amp	240	260	280
welding speed	cm/min	32	34	36
Nanoparticle	g	0.25	0.50	0.75

Table 1 Chemical compounds of base metal and filler wire

Chemical composition of AA5083 (wt%) weld plate									
Si	Ti	Ni	Zn	Cr	Mg	Mn	Cu	Fe	Al
0.145	0.0106	0.005	0.0861	0.0573	4.21	0.426	0.0561	0.285	Balance
Chemical composition of filler wire—AWS 5.10 ERS 183 (wt%)									
Si	Fe	Cu	Mn	Mg	Cr	Ti	Al		
0.4	0.40	0.1	0.5–1	4.3–5.2	0.057	0.15	Balance		

of nanoparticles inside the created groove, and the welding operation was performed.

4 Results and discussion

4.1 Investigation of input parameters

In this study, using the Taguchi technique, the parameters of current intensity, welding speed, and the amount of siliconized Zn-graphene oxide complex nanoparticles in three levels were coded as input parameters, and the variables geometrical of weld bead, including penetration depth, bead height, and bead width were considered as output process parameters were measured. The S/N and analysis of variance (ANOVA) analyses were done to establish the relationship between input parameters and output variables. ANOVA aims to evaluate the impact of input parameters on penetration depth, bead height, and bead width. It gives a clear image of how far the input parameter affects the output characteristics and the impact rate of each factor. Furthermore, ANOVA can be performed to see which process parameter is statistically significant for each quality characteristic. In addition, the S/N approach is utilized by the Taguchi technique to measure the deviations of quality characteristics from the desired value. The S/N ratio is the ratio of "Signal," representing the desirable value and the mean of output characteristics, and the "noise," representing the undesirable value and squared deviation of the output characteristics [33–36]. The penetration depth values measured based on the test design matrix are shown in Table 3. Figure 1 also shows the effect of the three parameters of current intensity, welding speed, and the nanoparticle amount on the penetration depth. According to the results shown in the graphs of Fig. 1, if the current intensity was in level one with the value of 240 amps, the welding speed should be in level three with a value of 36 cm.min^{-1}, and the nanoparticle amount in level one with the value of 0.25 g, it will be possible to obtain a weld bead with the highest penetration depth. On the one hand, as shown in the analysis of variance table (Table 4), the current intensity parameter had the slightest effect, and the nanoparticle amount had the most significant impact on the penetration depth. In such a way that level 1 of the nanoparticle's parameter, with the amount of 0.25 g, will have the highest penetration depth, and in the second level, with the amount of 0.5 g, the penetration depth will be reduced, and finally, in level 3, with the amount of 0.75 g of nanoparticles, the penetration depth will be the lowest. Also, regarding the welding speed parameter in terms of cm.min-1, it can be stated that with the increase in the welding speed of the electrode, the penetration depth first decreased and then increased. Finally, at a rate of 36 cm/min, the maximum value of the penetration depth was reached. The degree of influence this parameter was about 17% on the penetration depth in the welding samples.

Table 3 Orthogonal array for L9 with response for penetration depth (mean value and S/N ratio)

Array type: L-9	Current intensity (amp)	Welding speed (cm/min)	Nano-particle (g)	Penetration dept	
				Mean value	S/N ratio
L1	1	1	1	8.9	S/N ratio
L2	1	2	2	7.8	18.987
L3	1	3	3	8.2	17.841
L4	2	1	2	7.8	18.276
L5	2	2	3	7.4	17.841
L6	2	3	1	8.9	17.384
L7	3	1	3	7.4	18.987
L8	3	2	1	8.3	17.384
L9	3	3	2	8	18.381

Table 5 shows the measured values of the bead height in the welded samples based on Taguchi's design and the mean value and S/N ratio. Figure 2 shows the effects of current intensity, welding speed, and nanoparticle amount on the bead height. According to the results, if the current intensity and the nanoparticle amount are at level one and the welding speed is equal to 36 cm.min^{-1}, we will have a weld with the lowest bead height value. According to the variance analysis table (Table 6), the nanoparticle amount was the most influential factor on the bead height, in such a way that the bead height decreased by changing the nanoparticle amount from 0.25 g to 0.75 g. The nanoparticle amount in level one with 0.25 g will have the lowest bead height; in level three, with 0.75 g of nanoparticles, it will be the highest. On the other hand, by electing higher values of current intensity, the bead height increases, while increasing the welding speed has the opposite result, and increasing the welding speed decreases the bead height.

Table 7 shows the mean value and S/N ratio measured for the weld bead in the samples. Figure 3 also shows the graphs related to the effects of input parameters on the bead width as an output variable. The results show that increasing the current intensity from 240 amps at level one to 280 amps at level three has reduced the bead width. However, the results obtained regarding the welding speed were the opposite. Regarding the parameter of the nanoparticle amount, it can be concluded that level three with 0.75 g has a smaller bead width than 0.25 g and 0.5 g, so to have a weld bead with the smallest width, the current intensity on level three with a value of 280 amp, the value of welding speed should be placed at level one with a value of 32 cm.min^{-1} and the nanoparticle amount at level three with 0.75 g.

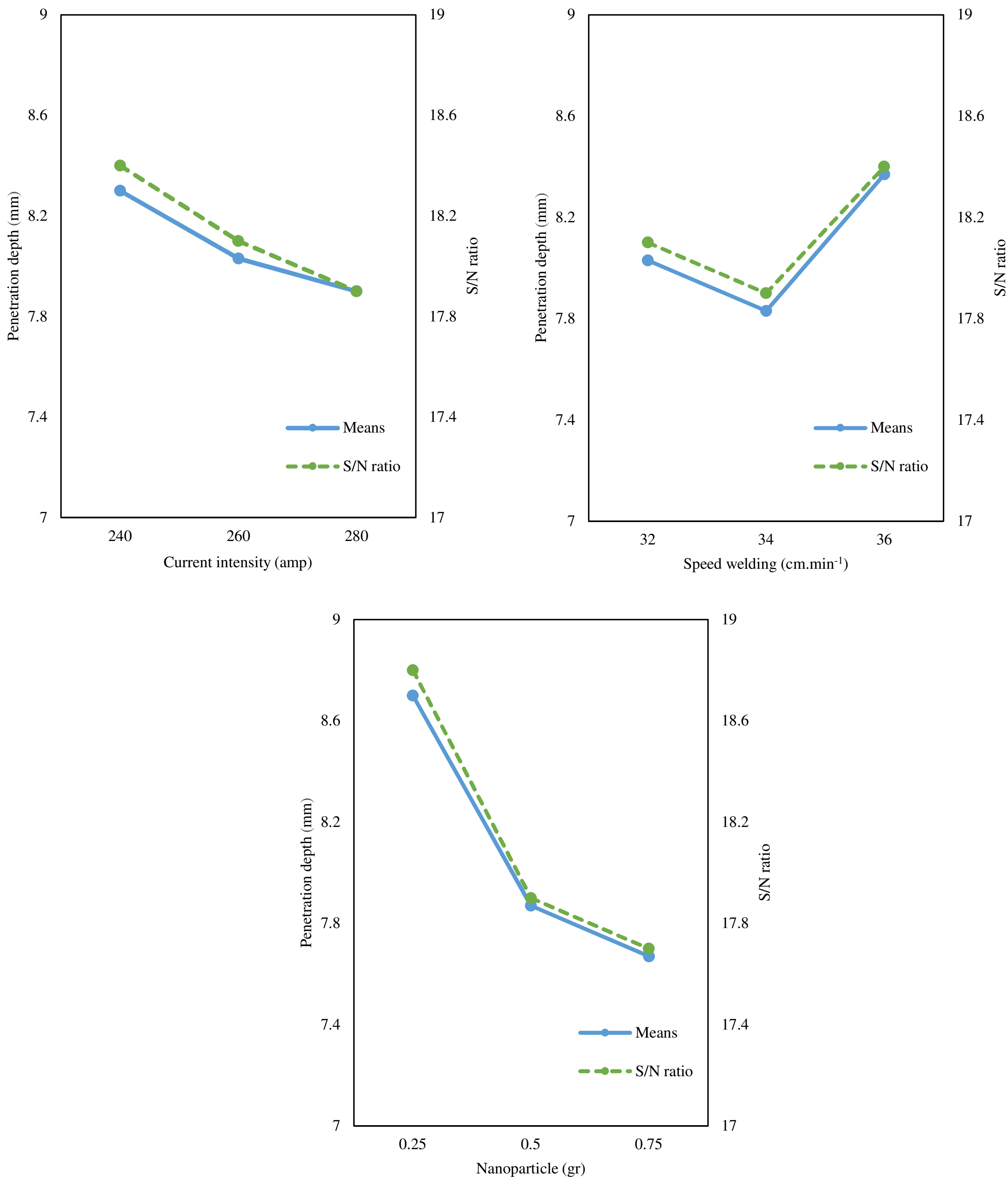

Fig. 1 Graphs related to the effect of process input parameters on the Penetration depth (mm)

Table 4 Analysis of Variance table for penetration depth

ANOVA for penetration depth (means)						
Factors	Degrees of freedom	Sums of squares	Adjusted mean square	Fisher ratio	Pure sum of squares	Percentage of Contribution
Current intensity	2	0.248	0.124	28.075	0.240	9.619
Welding speed	2	0.435	0.217	49.123	0.426	17.097
Nanoparticle	2	1.802	0.901	203.265	1.793	71.861
Other/Error	2	0.008	0.004	-	-	1.423
Total:	8	2.495				100%
ANOVA for penetration depth (S/N ratio)						
Current intensity	2	0.286	0.143	18.705	0.271	9.553
Welding speed	2	0.505	0.252	33.017	0.490	17.276
Nanoparticle	2	2.030	1.015	132.600	2.015	71.011
Other/Error	2	0.015	0.007	-	-	2.160
Total:	8	2.838				100%

Table 5 Orthogonal array for L9 with response for bead height (mean value and S/N ratio)

Array type: L-99	Current intensity (amp)	Welding speed (cm/min)	Nanoparticle (g)	Bead height	
				Mean value	S/N ratio
L1	1	1	1	1.6	4.082
L2	1	2	2	1.5	3.521
L3	1	3	3	2.1	6.444
L4	2	1	2	1.9	5.575
L5	2	2	3	2.4	7.604
L6	2	3	1	1.5	3.521
L7	3	1	3	3	9.542
L8	3	2	1	1.8	5.105
L9	3	3	2	1.85	5.343

4.2 Prediction of weld geometry

The S/N characteristics can be divided into three stages: nominal-the-better, smaller-the-better, and higher-the-better when the quality characteristics are continuous for engineering analysis. The higher-the-better and the smaller-the-better quality characteristics are employed in the welding process since this study aims to maximize the penetration depth and minimize the bead height and width through optimum process parameters. Therefore, in this research, the ideal weld was considered a weld with high penetration depth, low bead height, and width. Thus, according to the test results of the samples based on the test design matrix and the results obtained from the ANOVA and S/N statistical analyses, the objective function Bigger is better was considered. Therefore, to achieve the highest penetration depth, the input parameters of current intensity are set at level 1 with 240 amps, welding speed at level 3 with 36 cm.min^{-1}, and the amount of nanoparticles at level 1 with 0.25 g (Fig. 1). For the penetration depth, we can write:

$$\text{Penetration depth} = C\overline{S}_1 + T\overline{S}_3 + N\overline{S}_1 - 2\overline{T} \quad (1)$$

where $\overline{T}$ is the overall mean of penetration depth, 8.077 mm (Table 3); C $\overline{S}_1$ is the average penetration depth at first level of current intensity, 240 amp; T $\overline{S}_3$ is the average penetration depth at third level of welding speed, 36 cm.min^{-1}; N $\overline{S}_1$ is the average penetration depth at first level of nanoparticle, 0.25 g. By substituting these values in Eq. (1):

$$\begin{aligned} \textit{Penetration depth} &= 8.30 + 8.366 + 8.699 - (2 \times 8.077) \\ &= 9.211\ mm \end{aligned}$$

Also, considering the smaller is better function as the objective function to achieve the lowest bead height, the current intensity should be at level 1, the welding speed at level 3, and the nanoparticle amount at level 1 (Fig. 2), so we have:

$$\text{Bead height} = C\overline{S}_1 + T\overline{S}_3 + N\overline{S}_1 - 2\overline{T} \quad (2)$$

where $\overline{T}$ is the overall mean of bead height, 1.961 mm (Table 5); C $\overline{S}_1$ is the average bead height at first level of current welding, 240 amp; T $\overline{S}_3$ is the average bead height at third level of welding speed, 36 cm.min^{-1}; N $\overline{S}_1$ is the average bead height at first level of nanoparticle amount, 0.25 g. By substituting these values in Eq. (2):

$$\text{Bead height} = 1.733 + 1.816 + 1.633 - (2 \times 1.961) = 1.26\ \text{mm}$$

On the other hand, considering the smaller is better function as the objective function to achieve the smallest bead width, the current intensity in level 3 is 280 amps, the welding speed in level 1 is 32 cm.min^{-1}, and the nanoparticle

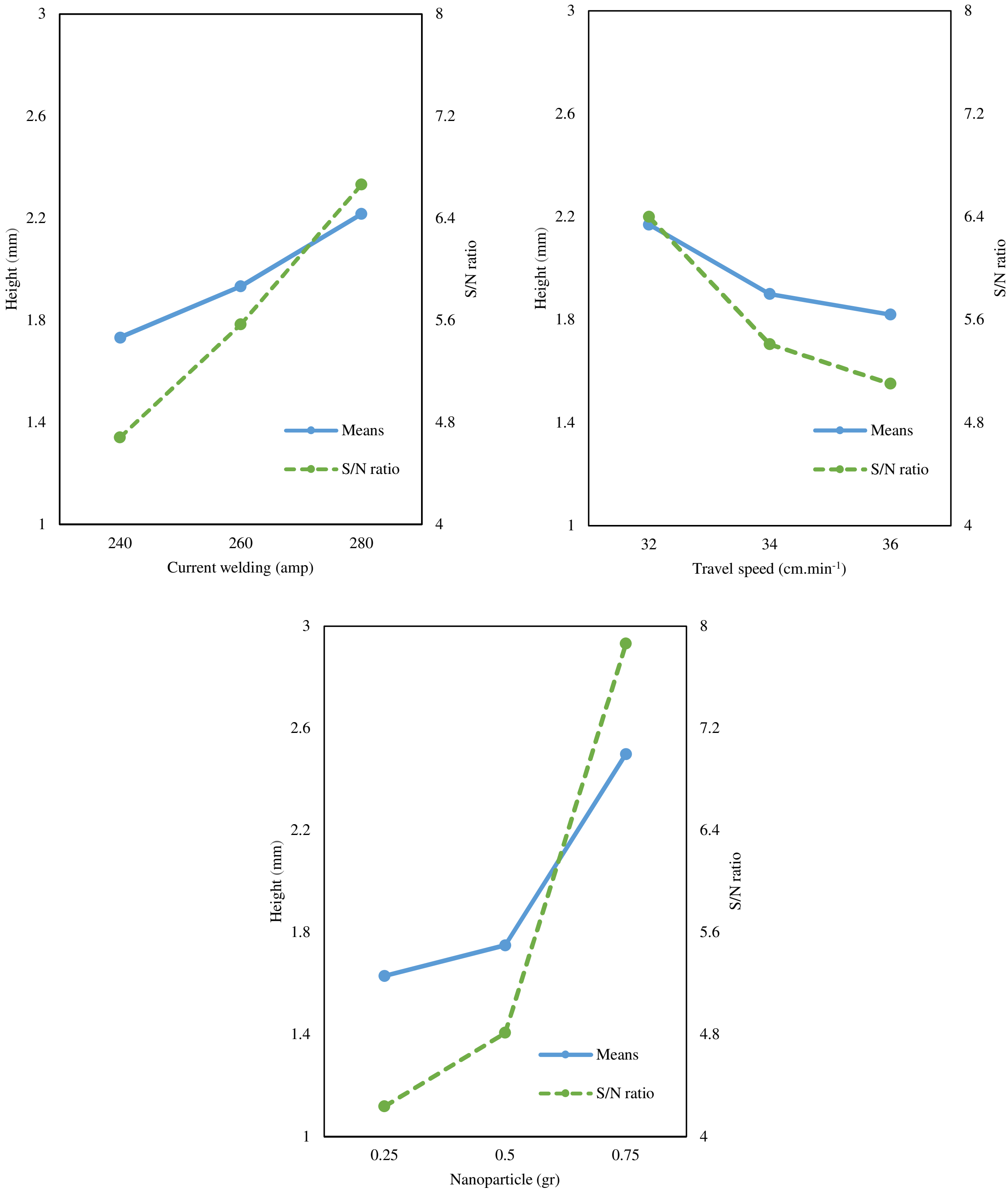

Fig. 2 Graphs related to the effect of process input parameters on the bead height

Table 6 Analysis of Variance table for bead height

ANOVA for bead height (means)						
Factors	Degrees of freedom	Sums of squares	Adjusted mean square	Fisher ratio	Pure sum of squares	Percentage of Contribution
Current intensity	2	0.353	0.176	48.994	0.346	18.352
Welding speed	2	0.200	0.100	27.765	0.193	10.235
Nanoparticle	2	1.327	0.663	183.747	1.319	69.882
Other/Error	2	0.006	0.003	-	-	1.531
Total:	8	1.888				100%
ANOVA for bead height (S/N ratio)						
Current intensity	2	5.908	2.954	107.172	5.853	18.575
Welding speed	2	2.755	1.377	49.971	2.699	8.567
Nanoparticle	2	22.792	11.396	413.427	22.737	72.156
Other/Error	2	0.054	0.027	-	-	0.702
Total:	8	31.511				100%

Table 7 Orthogonal array for L9 with response for bead width (mean value and S/N ratio)

Array type: L-9	Current intensity (amp)	Welding speed (cm/min)	Nano-particle (g)	Bead width	
				Mean value	S/N ratio
L1	1	1	1	11.2	20.984
L2	1	2	2	11.6	21.289
L3	1	3	3	11.1	20.906
L4	2	1	2	11	20.827
L5	2	2	3	9.8	19.824
L6	2	3	1	12	21.583
L7	3	1	3	9	19.084
L8	3	2	1	10.2	20.172
L9	3	3	2	10.9	20.748

amount in level 3 with a value of 0.75 g should be placed (Fig. 3), so we have:

$$\text{Bead width} = \mathrm{C}\overline{\mathrm{S}}_1 + \mathrm{T}\overline{\mathrm{S}}_3 + \mathrm{N}\overline{\mathrm{S}}_1 - 2\overline{\mathrm{T}} \tag{3}$$

where $\overline{\mathrm{T}}$ is the overall mean of bead width, 10.755 mm (Table 7); $\mathrm{C}\,\overline{\mathrm{S}}_{1}$ is the average bead width at third level of current intensity, 280 amp; $\mathrm{T}\,\overline{\mathrm{S}}_{3}$ is the average bead width at first level of welding speed, 32 cm.min^{-1}; $\mathrm{N}\,\overline{\mathrm{S}}_{1}$ is the average bead width at third level of nanoparticle amount, 0.75 g. By substituting these values in Eq. (3):

$$\text{Bead width} = 10.033 + 10.40 + 9.966 - (2 \times 10.755) = 8.889\ \text{mm}$$

So, to achieve the highest penetration depth and have a weld with the lowest bead height, the current intensity should be at level 1 with a value of 240 amps, the welding speed should be at level 3 with a value of 36 cm.min^{-1} and nanoparticle amount should also be put in level 1 with the amount of 0.25 g (Table 8).

On the other hand, considering the importance of achieving a higher penetration depth in addition to having a low bead height, in the investigation of the bead width variable, the current intensity at level 1, the speed Welding was used in level 3, and the nanoparticle amount was also used in level 1. The predicted sample (L00) was welded by setting the parameters of the current intensity, welding speed, and the nanoparticle amount. After the initial confirmation of the correctness of the weld in terms of possible defects, the variables of penetration depth, bead height, and bead width of the weld were measured. The investigations conducted on the weld sample L00 showed that this sample had a weld with a high penetration depth and a wide and low bead height in terms of weld bead appearance. Figures 4 and 5 show the cut sections of the weld metal's surface and the weld metal's surface. The results show that the bead height and width in the L00 sample had 1.30 mm and 12 mm values, respectively. In comparison, the predicted values for these variables were 1.260 mm and 8.889 mm, respectively. Also, according to the predicted penetration depth value, which was equal to 9.211 mm, the weld penetration depth in the L00 sample was 9.22 mm. Therefore, the measured penetration depth and bead height were very clearly similar to the predicted values. Further examination shows that the weld geometry in the L00 sample, which has 0.25 g of nanoparticles, compared to the welded sample without nanoparticles shown in Figs. 6 and 7, has a broader width but a lower bead height. In addition, in L00, the penetration depth increased significantly. Also, the shape of the arc during the welding operation in the L0 sample (Reference sample) was almost similar to a circle. In contrast, the L00 sample has

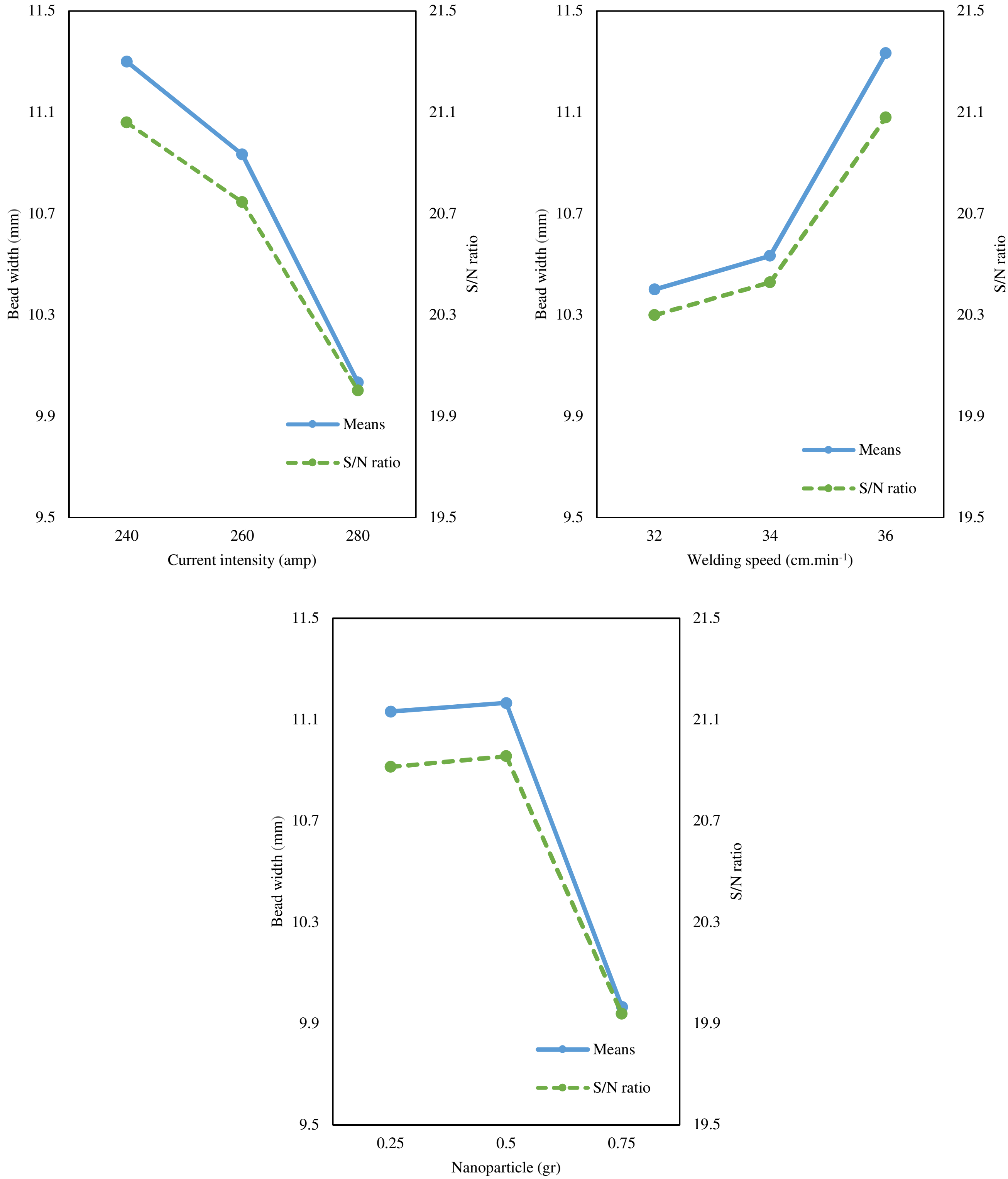

Fig. 3 Graphs related to the effect of process input parameters on the bead width

a concentrated and compressed arc. According to previous studies, the two factors of electric arc concentration and reversal of the Marangoni flow inside the molten pool due to the presence of surface-active elements such as oxygen [37, 38] can be among the main reasons for the increase in the penetration depth in the L00 sample.

Table 8 Analysis of Variance table for bead width

ANOVA for bead width (means)						
Factors	Degrees of freedom	Sums of squares	Adjusted mean square	Fisher ratio	Pure sum of squares	Percentage of Contribution
Current intensity	2	2.548	1.274	31.068	2.466	35.432
Welding speed	2	1.528	0.764	18.635	1.446	20.781
Nanoparticle	2	2.802	1.401	34.157	2.720	39.072
Other/Error	2	0.081	0.040	-	-	4.715
Total:	8	6.962				100%
ANOVA for bead width (S/N ratio)						
Current intensity	2	1.771	0.885	54.814	1.739	35.944
Welding speed	2	1.049	0.524	32.476	1.017	21.024
Nanoparticle	2	1.985	0.992	61.424	1.952	40.359
Other/Error	2	0.032	0.016	-	-	2.673
Total:	8	4.838				100%

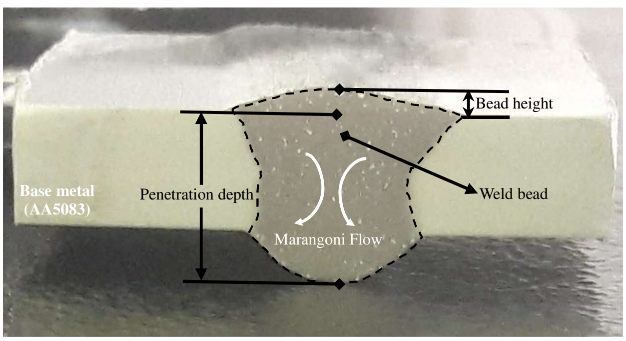

Fig. 4 Weld geometry and Marangoni flow of the welded sample with 0.25 g nanoparticles (L00)

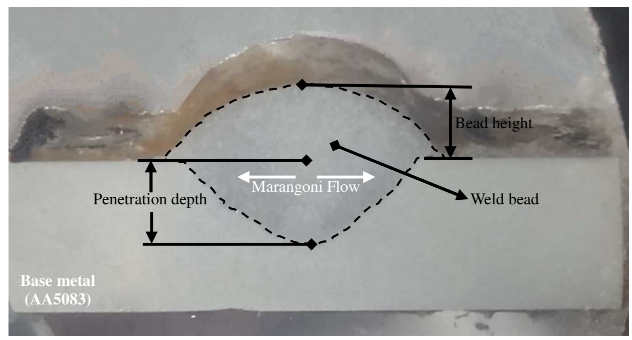

Fig. 6 Weld geometry and Marangoni flow of the welded sample with 0.00 g nanoparticles (L0)

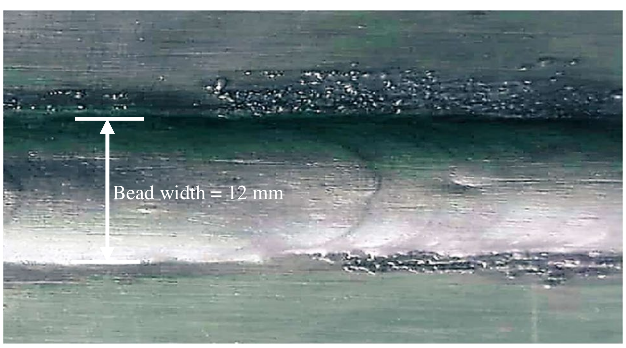

Fig. 5 Bead width of the welded sample with 0.25 g nanoparticles (L00)

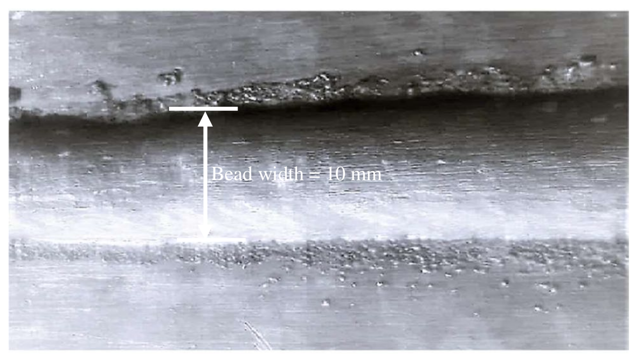

Fig. 7 Bead width of the welded sample with 0.00 g nanoparticles (L0)

4.3 Mechanical properties

The tensile test is a method to check the mechanical properties and determine the behavior of materials when axial tensile force is applied. The results determine the elastic and plastic range, elongation, ultimate tensile strength, and yield strength in different materials [39]. In this research, the tensile test was used to compare the mechanical properties of the welded parts. Therefore, from each of the L00 samples (welded with 0.25 g of nanoparticles) and L0 (welded sample without nanoparticles), three samples were extracted according to the ASTM-E8-sub size standard and tested by the SANTAM STM-600 traction machine. Figure 8 shows

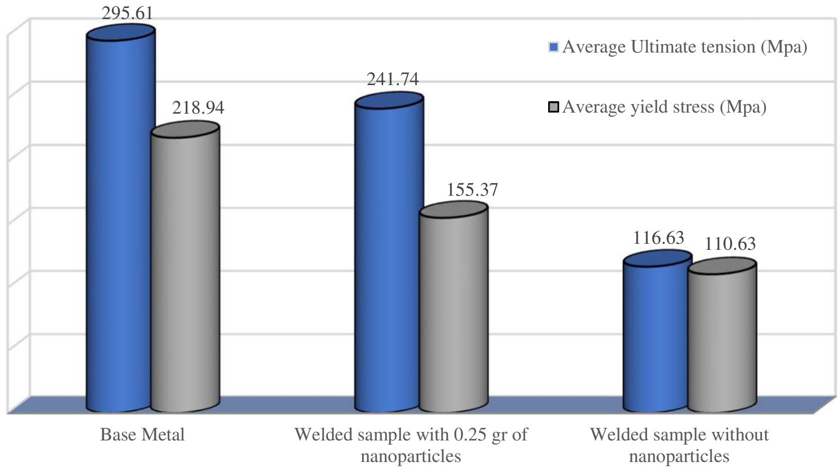

Fig. 8 The value of ultimate strength and yield strength in L00 samples (welded with 0.25 g of nanoparticles) and L0 (welded sample without nanoparticles)

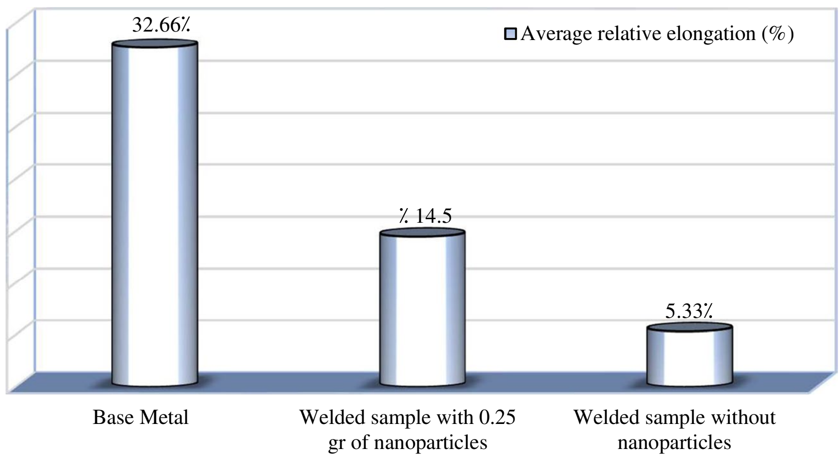

Fig. 9 The value of relative elongation in L00 samples (welded with 0.25 g of nanoparticles) and L0 (welded sample without nanoparticles)

the measured yield and ultimate strength values in two samples and compares them with base metal (AA5083). The results showed that in the L00 sample, the average ultimate tensile strength is 58.84%, and the yield stress is 28.24% higher than in the L0 sample. On the other hand, since the amount of tensile strength and yield strength represent the strength of the desired material, it can be concluded that the strength of the weld created in the L00 sample is generally higher than the weld sample without nanoparticles (L0). In addition, according to the comparison results of the relative length increase in the samples (Fig. 9), in the L00 sample, the relative length increase is 36.75% higher than in the L0 sample. Considering that the parameters of percentage increase in length and decrease in cross-sectional area indicate ductility, it can be concluded that the ductility of the L00 sample is also higher.

5 Conclusions

This study studied the effect of parameters of current intensity, welding speed, and the amount of siliconized Zn-graphene oxide complex nanoparticles on the welding geometry, including the variables of penetration depth, height, and bead width by the gas metal arc welding. Using the Taguchi method, the levels of the input parameters were determined, and the results obtained were checked by ANOVA and S/N analysis. The appropriate base of each parameter was determined to achieve welding with the highest penetration depth and low bead height. The results showed that:

- Conducting experiments and statistical analysis determined the optimal levels for each parameter, and the Taguchi technique predicted the welding geometry dimensions very well.

- The L00 sample had a smooth surface and no surface porosity or cavity. In addition, it had a weld with broad pollen, and its bead height was 1.3 mm, while the weld height in sample L0 equals 3 mm.
- The L00 sample has a weld with a high penetration depth, equal to 9.22 mm, while the maximum penetration depth in the L0 sample was 4.5 mm.
- In the L00 sample, the shape of the arc created due to the change in the direction of the Marangoni current due to the presence of the oxygen element was compact and almost bell-shaped. Still, in the welded sample without nanoparticles (L0), the arc created was circular.
- In the L00 sample, the average ultimate stress increased by 58.84%, the average yield stress increased by 28.24%, and the relative length increased by 36.75% compared to the L0 sample.

Supplementary Information The online version contains supplementary material available at https://doi.org/10.1007/s00170-024-13074-0.

Author Contributions All authors contributed to the study's conception and design. Material preparation, data collection, and analysis were performed by Farhad Rahmati. Masood Aghakhani designed and supervised the whole project and revised and analyzed data, and Farhad Kolahan analyzed and revised the manuscript. All authors read and approved the final manuscript. The authors would like to thank Dr. Eshagh Karimi, Dr. Shahab Zangeneh, Mr. Farzad Pahnaneh, and the Razi University of Kermanshah for their assistance throughout the research.

Funding The authors declare that no funds, grants, or other support were received during the preparation of this manuscript.

Declarations

Conflicts of Interest All authors declare that they have no conflicts of interest.

References

1. Messler RW Jr (2008) Principles of welding: processes, physics, chemistry, and metallurgy. Wiley (ISBN:3527617493, 9783527617494)
2. Houldcroft PT, John R (2001) Welding and cutting: A guide to fusion welding and associated cutting processes. Woodhead Publishing
3. DebRoy T, David SA (1995) Physical processes in fusion welding. Rev Mod Phys 67(1):85. https://doi.org/10.1103/RevModPhys.67.85
4. Jiang Z et al (2019) High efficiency and quality of multi-pass tandem gas metal arc welding for thick Al 5083 alloy plates. J Shanghai Jiaotong Univ (Sci) 24(2):148–157
5. Jia Y et al (2023) Current research status and prospect of metal transfer process control methods in gas metal arc welding. Int J Adv Manuf Technol 128(7–8):2797–2811
6. Rahmati F, Ghandehariun A (2023) Sustainability Development and Life Cycle Assessment of Welding Processes: Focus on SMAW and GMAW, In The 8th International and 19th National Conference on Manufacturing Engineering ICME2023
7. Katsas S, Nikolaou J, Papadimitriou G (2006) Microstructural changes accompanying repair welding in 5xxx aluminum alloys and their effect on the mechanical properties. Materials & Design 27(10):968–975. https://doi.org/10.1016/j.matdes.2005.02.012
8. Liang Y et al (2018) Effect of TIG current on microstructural and mechanical properties of 6061–T6 aluminum alloy joints by TIG–CMT hybrid welding. J Mater Process Technol 255:161–174. https://doi.org/10.1016/j.matdes.2005.02.012
9. Huang L et al (2018) Effect of the welding direction on the microstructural characterization in fiber laser-GMAW hybrid welding of 5083 aluminum alloy. J Manuf Process 31:514–522
10. Torzewski J et al (2020) Microstructure and low cycle fatigue properties of AA5083 H111 friction stir welded joint. Materials 13(10):2381
11. Mancha AEUA et al (2021) Experimental Study of Friction Stir Welding on Dissimilar Thickness of Aluminum Plate Butt Joints. Adv Eng Process Technol II:257–262
12. Bodaghi F, Atapour M, Shamanian M (2021) Assessment of microstructure and stress corrosion cracking susceptibility of multipass gas metal arc welded Al 5083–H321 aluminum alloy. Metallography Microstruct Anal 10(2):246–256
13. Ma M et al (2021) Effect of weld reinforcement on tensile and fatigue properties of 5083 aluminum metal inert gas (MIG) welded joint: Experiments and numerical simulations. Int J Fatigue 144:106046
14. Borrego L et al (2014) Fatigue life improvement by friction stir processing of 5083 aluminum alloy MIG butt welds. Theoret Appl Fract Mech 70:68–74
15. Liu Y et al (2012) Microstructure and mechanical properties of aluminum 5083 weldments by gas tungsten arc and gas metal arc welding. Mater Sci Eng, A 549:7–13
16. Verma RP, Pandey K (2021) Multi-response optimization of process parameters of GMA welding of dissimilar AA 6061–T6 and AA 5083-O aluminum alloy for optimal mechanical properties. Mater Today: Proc 46:10204–10210
17. Zhu C et al (2018) Molten pool behaviors and their influences on welding defects in narrow gap GMAW of 5083 Al-alloy. Int J Heat Mass Transf 126:1206–1221
18. Makhtar MF et al (2021) An Experimental Study on Friction Stir Welding of AA5083 Tee Lap Joints. Adv Eng Process Technol II:279–286
19. Rahmati F, Aghakhani M, Kolahan F (2023) Influence of Siliconized Zn-Graphene Oxide Complex Nanoparticles on the Microstructure and Mechanical Properties of AA5083: Focus on Gas Metal Arc Welding. Adv Mater Sci Eng
20. Fattahi M et al (2014) Improved microstructure and mechanical properties in gas tungsten arc welded aluminum joints using graphene nanosheets/aluminum composite filler wires. Micron 64:20–27. https://doi.org/10.1016/j.micron.2014.03.013
21. Khosravi M, Mansouri M, Gholami A, Yaghoubinezhad Y (2020) Effect of graphene oxide and reduced graphene oxide nanosheets on the microstructure and mechanical properties of mild steel jointing by flux-cored arc welding. Int J Miner Metall Mater 27(4):505–514. https://doi.org/10.1007/s12613-020-1966-7
22. Maurya R et al (2016) Effect of carbonaceous reinforcements on the mechanical and tribological properties of friction stir processed Al6061 alloy. Mater Des 98:155–166
23. Aghakhani M, Naderian P (2015) Modeling and optimization of dilution in SAW in the presence of Cr2O3 nano-particles. Int J Adv Manuf Technol 78(9):1665–1676
24. Aghakhani M et al (2014) Combined effect of TiO2 nanoparticles and input welding parameters on the weld bead penetration in submerged arc welding process using fuzzy logic. Int J Adv Manuf Technol 70(1):63–72

25. Razak MAAA et al (2021) Experimental Study on Self-Supported Friction Stir Welding on AA5083 Plate Butt Joints. Adv Eng Process Technol 2:293–298
26. Asadi P et al (2016) Optimization of AZ91 friction stir welding parameters using Taguchi method. Proc Inst Mech Eng Part L: J Mater: Des Appl 230(1):291–302
27. Odinikuku WE, Udumebraye JE, Atadious D (2020) Prediction of Weld Bead Geometry of Mild Steel Using Taguchi Technique and Multiple Regression Analysis. J Eng Res Rep 13(4):31–46
28. Datta S, Bandyopadhyay A, Pal PK (2008) Grey-based Taguchi method for optimization of bead geometry in submerged arc bead-on-plate welding. Int J Adv Manuf Technol 39:1136–1143
29. Ghosh N, Pal PK, Nandi G (2016) Parametric optimization of MIG welding on 316L austenitic stainless steel by grey-based Taguchi method. Procedia Technol 25:1038–1048
30. Lakshminarayanan AK, Balasubramanian V (2008) Process parameters optimization for friction stir welding of RDE-40 aluminium alloy using Taguchi technique. Trans Nonferrous Metals Soc China 18(3):548–554
31. Kechagias JD et al (2020) A comparative investigation of Taguchi and full factorial design for machinability prediction in turning of a titanium alloy. Measurement 151:107213
32. Meena A et al. (2018) Investigation of wear characteristics of dental composites filled with nanohydroxyapatite and mineral trioxide aggregate. Fundamental Biomaterials: Polymers. Woodhead Publishing, 287–305
33. Thakur AG et al (2010) Application of Taguchi method for resistance spot welding of galvanized steel. ARPN J Eng Appl Sci 5(11):22–26
34. Mohamed MA, Manurung YH, Berhan MN (2015) Model development for mechanical properties and weld quality class of friction stir welding using multi-objective Taguchi method and response surface methodology. J Mech Sci Technol 29:2323–2331.https://doi.org/10.1007/s12206-015-0527-x
35. Nandagopal K, Kailasanathan C (2016) Analysis of mechanical properties and optimization of gas tungsten Arc welding (GTAW) parameters on dissimilar metal titanium (6Al4V) and aluminium 7075 by Taguchi and ANOVA techniques. J Alloy Compd 682:503–516
36. Anawa EM, Olabi AG (2008) Using Taguchi method to optimize welding pool of dissimilar laser-welded components. Opt Laser Technol 40(2):379–388
37. Fujii H et al (2008) Effect of Oxygen Content in He-O_2 Shielding Gas on Weld Shape in Ultra Deep Penetration TIG. Trans JWRI 37(1):19–26
38. Yuri T et al (2001) Effect of welding structure on high-cycle and low-cycle fatigue properties for MIG welded A5083 aluminum alloys at cryogenic temperatures. Cryogenics 41(7):475–483
39. Wu L et al (2022) The microstructure and mechanical properties of 5083, 6005A and 7N01 aluminum alloy gas metal arc-welded joints for the high-speed train: A Comparative Study. Metals 12(2):213

Publisher's Note Springer Nature remains neutral with regard to jurisdictional claims in published maps and institutional affiliations.